PCCP

PAPER

View Article Online
View Journal | View Issue



Cite this: *Phys. Chem. Chem. Phys.*, 2016, **18**, 30462

# Giant spin–orbit effects on $^{1}$H and $^{13}$C NMR shifts for uranium(VI) complexes revisited: role of the exchange–correlation response kernel, bonding analyses, and new predictions†

Anja H. Greif,[a] Peter Hrobárik,*[a] Jochen Autschbach[b] and Martin Kaupp*[a]

Received 5th September 2016,
Accepted 18th October 2016

DOI: 10.1039/c6cp06129j

www.rsc.org/pccp

Previous relativistic quantum-chemical predictions of unusually large $^{1}$H and $^{13}$C NMR chemical shifts for ligand atoms directly bonded to a diamagnetic uranium(VI) center (P. Hrobárik, V. Hrobáriková, A. H. Greif and M. Kaupp, *Angew. Chem., Int. Ed.*, 2012, **51**, 10884) have been revisited by two- and four-component relativistic density functional methods. In particular, the effect of the exchange–correlation response kernel, which had been missing in the previously used two-component version of the Amsterdam Density Functional program, has been examined. Kernel contributions are large for cases with large spin–orbit (SO) contributions to the NMR shifts and may amount to up to ~30% of the total shifts, which means more than a 50 ppm difference for the metal-bonded carbon shifts in some extreme cases. Previous calculations with a PBE-40HF functional had provided overall reasonable predictions, due to cancellation of errors between the missing kernel contributions and the enhanced exact-exchange (EXX) admixture of 40%. In the presence of an exchange–correlation kernel, functionals with lower EXX admixtures give already good agreement with experiments, and the PBE0 functional provides reasonable predictive quality. Most importantly, the revised approach still predicts unprecedented giant $^{1}$H NMR shifts between +30 ppm and more than +200 ppm for uranium(VI) hydride species. We also predict uranium-bonded $^{13}$C NMR shifts for some synthetically known organometallic U(VI) complexes, for which no corresponding signals have been detected to date. In several cases, the experimental lack of these signals may be attributed to unexpected spectral regions in which some of the $^{13}$C NMR shifts can appear, sometimes beyond the usual measurement area. An extremely large uranium-bonded $^{13}$C shift above 550 ppm, near the upper end of the diamagnetic $^{13}$C shift range, is predicted for a known pincer carbene complex. Bonding analyses allow in particular the magnitude of the SO shifts, and of their dependence on the functional, on the ligand position in the complex, and on the overall electronic structure to be better appreciated, and improved confidence ranges for predicted shifts have been obtained.

## Introduction

The presence of a heavy element in a molecule may affect the nuclear magnetic resonance (NMR) chemical shifts of neighbouring atoms through spin–orbit (SO) effects.[1,2] These "SO chemical shifts" or "heavy-atom-effects on the light-atom shift" (HALA)[1] may alter the NMR shifts of certain nuclei in a system dramatically. As the SO shifts are mainly transmitted by a Fermi-contact-type mechanism,[3,4] atoms featuring a high s-orbital character in the bond towards the heavy-atom substituent are affected most significantly. Consequently, $^{1}$H shifts are most susceptible to SO-induced effects. Spectacular examples for low-frequency SO $^{1}$H shifts include the hydrogen halides[5,6] and in particular 4d or 5d transition-metal hydride complexes with $d^6$ or $d^8$ configurations,[7,8] with shifts down to −60 ppm *vs.* tetramethylsilane (TMS) for certain iridium complexes.[9] In contrast, the largest experimentally confirmed high-frequency $^{1}$H SO shifts so far are induced for metal hydrides with $d^{10}$ and $d^0$ configurations,[7,10–12] with measured shift values up to *ca.* +20 ppm.[13] The SO origin of many of these shifts has been confirmed by a large variety of quantum-chemical studies,

[a] *Institut für Chemie, Technische Universität Berlin, Strasse des 17. Juni 135, D-10623 Berlin, Germany. E-mail: peter.hrobarik@tu-berlin.de, martin.kaupp@tu-berlin.de*
[b] *Department of Chemistry, University at Buffalo, State University of New York, Buffalo, NY, 14260, USA*

† Electronic supplementary information (ESI) available: NMR chemical shifts of U(VI)-bound ligand atoms computed at DFT level using various EXX admixtures and different structures, their decomposition into individual (diamagnetic, paramagnetic and spin–orbit) terms, NMR shift tensor anisotropies, detailed bonding analysis and Cartesian coordinates of optimized structures. See DOI: 10.1039/c6cp06129j

ranging from a perturbational treatment of SO coupling *via* two-component quasirelativistic approaches to fully relativistic four-component calculations, using in most cases density functional theory (DFT) methods.[2,3,5,12,14,15]

Using two-component ZORA ("zeroth-order regular approximation")[16,17] relativistic calculations, we have recently predicted spectacular SO-induced high-frequency $^{1}$H and $^{13}$C shifts in actinide complexes with $5f^0$ configuration, in particular for uranium(VI) species.[12] The predicted $^{1}$H chemical shifts of suitable target U(VI) hydride complexes ranged up to clearly beyond +100 ppm, which would considerably extend the known $^{1}$H shift range for diamagnetic compounds. As the computed shifts depended strongly on the exact-exchange (EXX) admixture of the DFT exchange–correlation functional, in the absence of experimental $^{1}$H data our strategy for the selection of the most suitable functional was based on the parallel study of $^{13}$C shifts in uranium(VI) organometallic complexes. In the latter case, some experimental data were available, and the evaluation of functionals on these data suggested best performance for a PBE-based global hybrid functional with 40% EXX admixture (PBE-40HF).[12] Values obtained with this functional were then put forward as predictions for the unknown $^{1}$H chemical shifts in U(VI) hydride complexes,[12] and for the $^{13}$C NMR shifts in two new U(VI) alkyl complexes.[18] The predictions in the latter cases were subsequently confirmed experimentally, resulting in one case in the drastic revision of a previous experimental assignment.[18]

However, recent findings regarding the two-component ZORA implementation for NMR shifts in the ADF program,[19] which had been used for our studies on actinide systems, suggest that we may have obtained the right answer for not entirely the right reasons: One of us noted that the ADF NMR shielding implementation misses the linear response of the exchange–correlation potential (*i.e.* the shielding contribution from the response XC kernel) to the external perturbation.[20] It was argued by Wolff and Ziegler in the publication preceding the one reporting the original ZORA NMR implementation that this shielding contribution 'even for heavy atoms [is] not large'.[16] This is indeed not a problem in the absence of significant SO effects, as the perturbation operators for external magnetic field and nuclear magnetic moment are imaginary ones that do not create coupling terms for pure (semi-)local functionals. However, due to the impact of the electron spin-dependent part of the hyperfine interaction (a real perturbation) for the SO nuclear shielding effects (see above), the kernel becomes important or even essential in cases of large SO contributions when using spin-polarized calculations.[21] Employing a modified pilot implementation, Autschbach demonstrated significant changes between the standard implementation in ADF and the modified one for $^{1}$H shifts in hydrogen halides and for $^{199}$Hg shifts in mercury halides were demonstrated.[20] Notable differences between two- and four-component results in a recent study of carbon and nitrogen shifts in transition-metal cyanide complexes also pointed to possible inaccuracies with the previous ZORA implementation in ADF due to the lack of the XC-kernel SO effects on the nuclear magnetic shielding[22] (see also ref. 15 and 23 for other two- *vs.* four-component comparisons). Even more recently, we have compared both the original and the modified implementation to four-component calculations for $^{1}$H and $^{195}$Pt shifts in a series of platinum hydride complexes.[14] While absolute shieldings at two-component ZORA and four-component levels differed considerably (as has been shown earlier in other cases[24]), the relative shifts agreed rather well, provided the XC-kernel SO contributions were included at both levels, and excellent agreement with the experimental shifts was obtained with PBE0. The effects of the missing XC contributions were large and excellent agreement with the experimental values was found with PBE0. In another recent study of $^{13}$C and $^{15}$N shifts in similar square-planar transition-metal complexes, the missing kernel in the standard ADF implementation was again successfully compensated for by 40% EXX admixture to the functional.[15]

In view of these observations, in this work we re-evaluate our previous calculations on $^{1}$H and $^{13}$C shifts in uranium(VI) complexes, using the modified two-component ZORA implementation in ADF in comparison with four-component Dirac–Kohn–Sham (DKS) calculations. In spite of some uncertainties concerning reproducibility of experimental data, it turns out that upon inclusion of the XC response kernel in the NMR calculations, the optimal EXX admixture needed for best agreement with the abovementioned experimental $^{13}$C shifts is often considerably lower than the *ca.* 40% needed without kernel (see above). In the end, a conventional PBE0 functional with 25% EXX admixture seems to be a reasonable choice for the NMR shift calculations of uranium(VI) complexes, tending to somewhat overestimate $^{13}$C NMR shifts. Calculations using PBE0 or related functionals with inclusion of the exchange–correlation kernel also confirm the overall range of the predicted spectacular high-frequency $^{1}$H shifts in U(VI) hydride complexes, although with some modifications of the detailed predicted values in either direction. Moreover, calculated $^{13}$C shifts for other recently synthesized organometallic uranium(VI) complexes are reported, extending the spectral range for uranium-bonded carbon shifts from about 20 ppm to above 550 ppm.

## Computational details

We have performed gas-phase structure optimizations with the Turbomole program[25] using def2-TZVP basis sets[26,27] and the Perdew–Burke–Ernzerhof (PBE)[28] functional within the generalized gradient approximation (GGA), its hybrid form (PBE0),[28,29] and with B3LYP.[30,31] This computational level includes a small-core (60 core electrons) quasi-relativistic effective-core potential (ECP) for uranium.[26] In addition, atom-pairwise corrections for dispersion forces were simulated *via* Grimme's D3 model with Becke–Johnson (BJ) damping.[32,33] The quality of the optimized structures was evaluated by comparison of metal–ligand bond lengths (in particular U–C bonds) with experiment, where available.

The two-component quasirelativistic ZORA[16,17] DFT calculations have been carried out using the Amsterdam Density Functional (ADF) program[19] with the PBE functional,[28] and with PBE-based hybrids having variable EXX admixture,[34,35] using all-electron Slater-type orbital basis sets of triple-ζ doubly polarized (TZ2P)[36]

quality, and an integration accuracy of 5.0 (Voronoi grids). The calculations used gauge-including atomic orbitals (GIAOs).[37] The ZORA calculations of NMR chemical shifts are done with and without the previously neglected terms from the exchange–correlation (XC) response kernel.[20] We note in passing that the implementation of the PBE functional used here without and with XC kernel differs slightly, as the former uses PW92[29] for the LDA part and the latter VWN.[38] The latter goes back to the initial implementation of PBE in ADF by S. Patchkovskii. However, the differences affect the results negligibly.

Bulk solvent effects on the optimized structures and on the computed NMR shieldings were simulated *via* the conductor-like screening model (COSMO),[39–41] both in Turbomole and in ADF.

For comparison, fully relativistic four-component GIAO-DFT calculations at the matrix Dirac–Kohn–Sham (mDKS) level of theory and Gaussian-type orbital basis sets have been performed with the ReSpect program package.[42] The approach uses restricted magnetically balanced (RMB) orbitals for the small component[43,44] and includes a correct XC kernel treatment (which can be turned off for testing and comparison). The mDKS calculations have been done at generalized-gradient-approximation level with the PBE functional.[28,45] For the uranium center, Dyall's all-electron valence-triple-ζ (Dyall TZ)[46] basis set has been employed, together with fully uncontracted Huzinaga–Kutzelnigg-type IGLO-III basis sets[47] for the ligand atoms.

The calculated $^{1}$H and $^{13}$C nuclear shieldings $\sigma$ were converted to chemical shifts $\delta$ (in ppm) relative to the shielding of TMS, computed at the same level. The SO contributions to the $^{13}$C chemical shift were computed as $\delta^{SO} = 0.9\ \text{ppm} - \sigma^{SO}$, where the value of 0.9 ppm corresponds to the SO part of the isotropic $^{13}$C shielding in TMS.

Analysis of natural localized molecular orbitals (NLMOs) at the scalar relativistic level was done with the NBO 5.9 module in Gaussian09 (G09)[48] using def(2)-TZVP[27,49] basis sets and the corresponding small-core ECP for uranium.[26,50] Interestingly, we noted problems with the NBO 5.0 module in the ADF 2012 package[51] when applied to uranium complexes. Without an error message, strongly overestimated f-orbital and underestimated d-orbital contributions to the U–C bonds were found compared to the G09 results, whereas no problems for transition-metal complexes were observed (*cf.* Table S1 in ESI†). In contrast, NBO 6.0 in ADF (2014)[52] gave data in good agreement with the G09 results. We thus suspect erroneous NBO analysis for f-element compounds in the older NBO version that comes with ADF. The delocalization index (DI), as a measure of shared electrons (bond covalency) between two atoms in question in the context of the quantum theory of atoms-in-molecules (QTAIM),[53,54] was calculated with the Multiwfn program,[55,56] at the same level as used for NLMO analyses (the corresponding .wfx files were generated in G09).

# Results and discussion

### Evaluation of the quality of the optimized structures

As chemical shifts can be very structure-dependent, a meaningful benchmarking of methods for shift calculations relies on accurate input structures. We therefore scrutinize initially the optimized structures of the organometallic complexes used for computation of $^{13}$C shifts. Despite the recently described renaissance of non-aqueous uranium chemistry and, thus, of organouranium chemistry,[57] only a few complexes with direct U(VI)–C σ bonds were characterized structurally to date. $^{13}$C NMR shifts of these complexes are even scarcer. Thus, our evaluation of structures and carbon NMR shifts uses the same set of recent organometallic complexes investigated in our previous work (complexes **1–3**, **6**, **7**),[12] however, three additional systems are considered here (**4**, **5**, **8**) (*cf.* Fig. 1 for all these structures). The latter include complex **8** as an example for a number of known U(VI) complexes with a methanide ligand and chelating phosphorano (in this case thiophosphorano) arms.[58–60] These systems exhibit clearly smaller (low-frequency) $^{13}$C shifts (with a resonance peak at about 20 ppm) than the other complexes.

Fig. 2 plots percentage deviations of optimized uranium-carbon bond lengths from experiment at different theory levels, with and without including dispersion corrections (see Table S2 in ESI† for numerical data). A clear distance trend is found, where B3LYP and PBE give the largest and PBE0 and PBE0-D3 the lowest values (with differences between 0.04 and 0.09 Å). The B3LYP-D3 and PBE0-D3 structures feature the smallest standard deviation (Table S2, ESI†), also for the U–N and U=O bonds (Table S3, ESI†). While the rather short PBE0-D3 distances underestimate the pure σ-bond in **5** (by 0.05 Å), PBE0-D3 structures will be used in the following for the evaluation of $^{13}$C shifts. Note that PBE0 structures are known to perform excellently for transition-metal complexes, as has also been found in a recent systematic analysis.[15] Additional NMR shift calculations for the structures optimized at B3LYP-D3 level are also provided to estimate the influence of the structural differences on the chemical shifts (see below). Bulk solvent effects simulated *via* the conductor-like screening model (COSMO)[39–41] are found to be negligible for the structural parameters (Table S4, ESI†). In view of the large SO effects on NMR shifts, we also performed

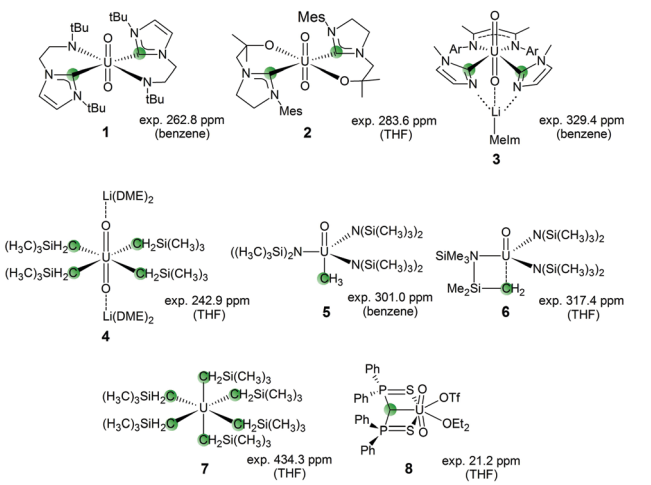


Fig. 1 Organometallic uranium(VI) complexes with known $^{13}$C NMR shifts for metal-bound carbon atoms (highlighted in green). See Table 3 for corresponding references.

 

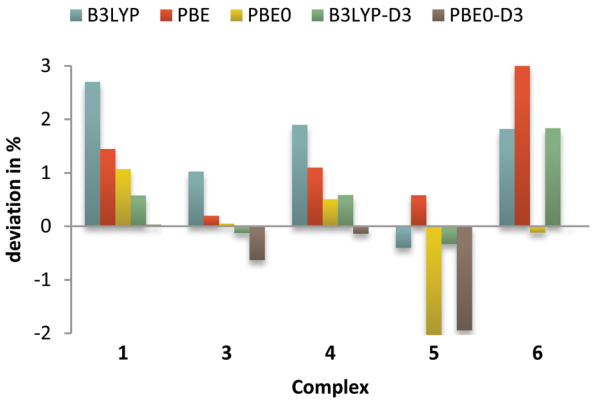


Fig. 2 Deviations from experiment of the U–C bond lengths optimized at different levels. See Table S2 in ESI† for numerical data and standard deviations. Average for two non-equivalent alkyl carbon atoms in **4** shown.

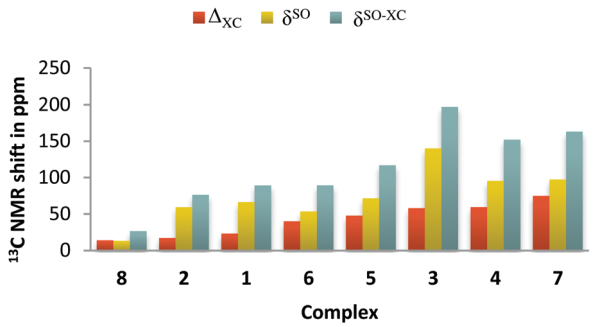


Fig. 3 Total XC-kernel contribution ($\Delta_{XC} = \delta^{xc}_{2c} - \delta_{2c}$) to the calculated $^{13}$C NMR shifts for complexes **1–8** in comparison with the SO shift contributions without ($\delta^{SO}$) and with ($\delta^{SO\text{-}XC}$) exchange–correlation kernel at PBE level; ordered by increasing $\Delta_{XC}$.

structure optimizations for selected complexes at the 2c-ZORA/TZ2P level with spin–orbit coupling. These calculations revealed rather minor 5f-SO effects on both U–C and U–H bond lengths, mostly smaller than 0.01 Å (*cf.* Table S5, ESI†).

### Interplay of functional and XC kernel contributions for the $^{13}$C shifts

Computed $^{13}$C NMR shifts of the carbon atoms directly bound to uranium in complexes **1–8** are presented in Table 1 (see also Fig. 1 and Table 3 for experimental data).

Starting with the effect of the kernel at PBE level, we see an appreciable increase of the $^{13}$C shifts upon inclusion of the kernel for all systems. The lowest impact ($\Delta_{XC}$ = 13.6 ppm) is observed for a methanide complex **8**, which exhibits also the smallest overall SO contribution to the $^{13}$C NMR shift. In fact, the influence of the kernel is connected to the magnitude of SO effects (*cf.* Fig. 3). Thus, for the σ-bonded carbon atoms in **4**, **5** and **7** (with $\delta^{SO}$ contributions of 115–165 ppm), the kernel contribution increases the shift by *ca.* 30%, which means 45–65 ppm difference for the carbon shift! For the N-heterocyclic carbene complexes **1** and **2** (with $\delta^{SO}$ contributions of *ca.* 75–90 ppm) the effect is below 10%. The "ate" complex **3** deviates slightly from this pattern as it exhibits the largest $\delta^{SO}$ contribution at PBE level but is only at third place in the XC kernel contribution.

Table 1 Computed isotropic $^{13}$C NMR shifts without and with kernel (in ppm *vs.* TMS) for uranium(VI)-bound carbon atoms. $\delta^{SO}$ contributions are given in parentheses[a]

| Complex | $\delta_{2c}$ (PBE) | | $\delta^{xc}_{2c}$ (PBE) | | $\delta_{2c}$ (PBE0) | | $\delta^{xc}_{2c}$ (PBE0) | |
|---|---|---|---|---|---|---|---|---|
| **1** | 266.4 | (66.2) | 289.4 | (89.1) | 270.6 | (62.5) | 286.8 | (78.6) |
| **2** | 283.5 | (59.1) | 300.4 | (76.1) | 288.5 | (52.1) | 299.5 | (63.1) |
| **3** | 360.1 | (139.9) | 417.9 | (197.0) | 347.6 | (130.6) | 387.3 | (169.9) |
| **4** | 174.2 | (95.3)[b] | 233.5 | (151.9)[b] | 209.3 | (134.6)[b] | 291.5 | (212.9)[b] |
| **5** | 184.1 | (71.4) | 231.7 | (116.8) | 231.6 | (107.6) | 299.9 | (172.8) |
| **6** | 207.3 | (53.3) | 247.1 | (89.2) | 253.7 | (82.7) | 313.7 | (137.4) |
| **7** | 249.0 | (97.2) | 323.7 | (163.0) | 340.5 | (181.2) | 536.8 | (363.5) |
| **8** | 38.9 | (12.9) | 52.6 | (26.3) | 22.1 | (7.3) | 28.5 | (13.4) |

[a] 2c-ZORA-SO/TZ2P results using PBE and PBE0 functional, respectively. Superscript "xc" indicates inclusion of the XC kernel. [b] Averaged data for two non-equivalent alkyl carbon atoms.

The total shielding is partitioned in the ADF output into a diamagnetic component that is calculated as an expectation value of a bilinear perturbation operator, and a linear response part that involves the perturbed Kohn–Sham orbitals to first order. The linear response part is further partitioned into a paramagnetic contribution that has a nonrelativistic counterpart, and a SO contribution involving the electron spin-dependent hyperfine operators that vanishes in the absence of SO coupling. The calculations confirm clearly the expectation that the kernel contribution affects almost exclusively the SO part of the nuclear shielding constants (*cf.* Tables S6 and S7 in ESI†). The paramagnetic part is influenced slightly as well (in particular for **7**, by about 10 ppm; see Tables S6 and S7, ESI†), as the first-order perturbed orbitals differ with and without consideration of the kernel.[61]

At first sight one would expect the kernel contribution to diminish when going from the "pure" GGA functional PBE to its hybrid form PBE0, as 25% of the PBE exchange have been replaced by exact exchange, and these 25% thus do not enter the kernel (the exact-exchange contributions are accurately accounted for in both implementations). While this expectation is borne out for the cases with relatively small kernel contributions (**1–3**, **8**), the kernel contribution actually increases with EXX admixture for **4–7**!

Strikingly, the latter four species are those complexes that exhibit a larger (more deshielded) $^{13}$C NMR shift with EXX admixture than without. This may be attributed to a mutual enhancement (cross terms) between EXX-derived coupling terms and the PBE kernel contributions within the generalized coupled-perturbed Kohn–Sham scheme used. Closer analysis (Tables S6 and S7, ESI†) confirms that it is mostly the SO contributions that account for these trends (with sizeable paramagnetic contributions for **7**, see above). The differences between XC kernel contributions at PBE and PBE0 levels correlate with the differences in the shifts for the two functionals. That is, large increases of the kernel contributions upon going from pure PBE to the hybrid functional are found for the cases with the overall largest shift increases with EXX admixture, and *vice versa*.

The largest SO effects and thus the largest kernel contributions tend to be found for complexes with the most pronounced

uranium 5f-orbital involvement in bonding (and thus particularly low-lying nonbonding unoccupied 5f-type orbitals).[12] We previously found a similar enhancement of the SO contributions with 5d-orbital contribution in the case of $^{1}$H shifts in platinum hydride complexes (in that case the SO effects are shielding, in contrast to the deshielding effects in the present work).[20] More detailed bonding analyses are provided below.

We note in passing that comparison of PBE0-D3 and B3LYP-D3 structures as input for the shift calculations without XC kernel changes the NMR shifts typically by only a few ppm, except for the very sensitive case of **7**, where somewhat larger effects of about 20 ppm (PBE0 shift calculation) are found (Table S8 in ESI†). Notably, these differences are enhanced by the kernel contribution. Use of B3LYP-D3 structures increases the shifts by about 20 ppm for complexes **4–6** but by 154 ppm for uranium(VI)-hexaalkyl **7**, which is also the system with the overall largest SO contributions. Interestingly, the shifts (and SO contributions) for the B3LYP-D3 optimized structures are larger (high-frequency shifted) even though the calculated U–C bonds are longer (*cf.* Fig. 2 and Table S2, ESI†). Intuitively, one might have expected the opposite trend, as the Fermi-contact mechanism for the SO-induced shift contributions should be enhanced for shorter distances.

Since the experimental NMR shifts were measured in organic solvents with varying polarity, such as pyridine-$d_5$ (**2**), benzene-$d_6$ (**1**, **3**, **5**) or THF-$d_8$ (**4**, **6–8**), we also evaluated the bulk solvent effects on computed NMR shifts. In general, these have somewhat larger influence when using functionals with a higher EXX admixture, as also observed in ref. 15. However, even with PBE0 and kernel, solvent effects on the NMR shifts obtained with the COSMO model tend to be below 7 ppm (Table S9 in ESI†).

Table 2 Comparison of computed 2- and 4-component $^{13}$C NMR shifts with and without kernel (in ppm *vs.* TMS) of uranium(VI)-bound carbon atoms in model complexes[a,b]

| Complex | $\delta_{2c}$ (PBE) | $\delta_{2c}^{xc}$ (PBE) | $\delta_{4c}$ (PBE) | $\delta_{4c}^{xc}$ (PBE) |
|---|---|---|---|---|
| **1′** | 270.3 | 293.2 | 275.0 | 299.7 |
| **5** | 184.1 | 231.7 | 184.5 | 232.8 |
| **7′** | 227.3 | 317.2 | 226.3 | 311.2 |
| **8′** | 15.4 | 23.3 | 17.1 | 26.5 |

[a] $\delta_{2c}$: 2c-ZORA-SO/TZ2P results; $\delta_{4c}$: 4c-mDKS results with Dyall TZ/IGLO-III basis. [b] **1′**: $^{t}$Bu group replaced by H; **7′**: $CH_2SiMe_3$ ligand replaced by $CH_3$; **8′**: Ph group replaced by H and $OEt_2$ replaced by $OMe_2$.

In addition to the two-component ZORA results discussed so far, Table 2 provides four-component (4c) mDKS results for some complexes. The standard 4c-mDKS implementation includes a correct XC kernel treatment, which can be turned off to get insight into the kernel contribution. 2c-ZORA results with ADF are given for comparison, as bulky substituent groups in **1**, **7**, and **8** had been replaced by smaller ones for the 4c-mDKS calculations (see footnotes in Table 2 for more details; complex **5** was taken without modification). The truncation in **1′** and **7′** has very small effects on the carbon shifts, whereas the $^{13}$C shift in **8** is about halved in **8′** (Table 1). The latter is mainly due to the almost 0.1 Å longer U–C distance in **8′** compared to **8** (*cf.* Table S2 in ESI†). The 4c-mDKS results are overall close to the 2c-ZORA results with and without kernel contributions, respectively, differing generally by less than 7 ppm. Thus, the importance of the kernel terms is very similar at 4c- and 2c-levels, consistent with previous results for transition-metal cyanide[22] and hydride complexes,[14] and with $^{199}$Hg relative shifts in ref. 23 (notwithstanding the fact that in the latter case absolute shieldings at 4c-mDKS and 2c-ZORA levels differed appreciably). The moderate differences between 2c- and 4c-results reflect technical differences between implementations (basis sets, grids, functionals, spin–orbit operators).

### Evaluation of the functional for $^{13}$C shift calculations

As seen in Table 1 and from our previous calibration without kernel,[12] the dependence of $\delta(^{13}C)$ on the functional does not provide a very clear-cut picture for the experimentally known uranium(VI) complexes. Table 3 provides the $^{13}$C NMR shifts obtained with kernel, using EXX admixtures of 0% (PBE), 10%, 15%, 25% (PBE0) and 40% for complexes **1–8** in comparison with experiment. For the N-heterocyclic carbene (NHC) complexes **1–3**, dependence on EXX admixture is relatively weak (below 10 ppm with a non-monotonous trend for **1** and **2**, up to 60 ppm for **3**). This is mainly caused by a decrease of the absolute value of the SO contributions with increasing EXX admixture (in contrast to the increase for **4–7**) while the paramagnetic contributions increase by comparable amounts for **1** and **2** and remain almost constant for **3** (Tables S6 and S7 in ESI†). The behaviour for the methanide complex **8** is similar as for **3**.

Our previous validation of functionals without kernel in ref. 12, which provided PBE-40HF as the best-performing functional,

Table 3 Dependence of $^{13}$C NMR shifts (in ppm *vs.* TMS) of uranium(VI)-bound carbon atoms on EXX admixture for structures optimized on PBE0-D3/def2-TZVP level[a]

| Complex | $\delta_{2c}^{xc}$ (PBE) | $\delta_{2c}^{xc}$ (PBE-10HF) | $\delta_{2c}^{xc}$ (PBE-15HF) | $\delta_{2c}^{xc}$ (PBE0) | $\delta_{2c}^{xc}$ (PBE-40HF) | $\delta_{2c}$ (PBE-40HF) | $\delta_{exp}$ |
|---|---|---|---|---|---|---|---|
| **1** | 289.4 | 290.0 | 289.4 | 286.8 | 280.5 | 270.3 | 262.8[62] |
| **2** | 300.4 | 300.7 | 300.4 | 299.5 | 297.3 | 290.5 | 283.6[63] |
| **3** | 417.9 | 409.8 | 403.6 | 387.3 | 360.0 | 334.2 | 329.4[64] |
| **4** | 233.5[b] | 257.5[b] | 268.5[b] | 291.5[b] | 306.9[b] | 230.6[b] | 242.9[18] |
| **5** | 231.7 | 257.5 | 270.6 | 299.9 | 362.2 | 277.4 | 301.0[65] |
| **6** | 247.1 | 271.7 | 284.3 | 313.7 | 373.3 | 296.8 | 317.4[66] |
| **7** | 323.7 | 377.5 | 418.0 | 536.8 | 936.0 | 489.0 | 434.3[18] |
| **8** | 52.6 | 41.7 | 37.1 | 28.5 | 17.4 | 14.8 | 21.2[59] |

[a] 2c-ZORA-SO/TZ2P results. Superscript "xc" indicates inclusion of the exchange–correlation kernel. [b] Averaged data for two non-equivalent alkyl carbon atoms.

 

was essentially based on the $^{13}$C shifts of **1–3** and **6**. As the results for **1** and **2** depend relatively little on the EXX admixture (*cf.* Table 3), the good performance for **3** and **6** was decisive for the choice of "best" functional in that case. Uranium hexaalkyl complex **7** was found to have been misassigned previously,[67] and its actinide-bound carbon shift was predicted in ref. 12. A subsequent re-measurement of **7** reported in ref. 18 showed that PBE-40HF level without kernel had predicted the general spectral region correctly but still overestimated this remarkably high-frequency shift (Table 3) by about 100 ppm (much closer $^{13}$C shift value of 436.5 ppm was achieved upon shortening of the U–C bond by 0.01 Å when including dispersion corrections in the structure optimization and using PBE-35HF with 35% EXX instead of PBE-40HF).[18] In that work the new complex **4** was reported, and its "blind test" assignment gave very good agreement between the PBE-40HF carbon shift (using PBE0/def-TZVPP structure) and experiment. The surprisingly good performance of PBE-40HF without kernel for **1–4** and **6** and the overestimate for **7** are documented in Table 3. The rather small experimental database of U(VI)-bound carbon atoms with significant dependence on EXX admixture did not allow a more accurate calibration without kernel contribution in ref. 12, and it hinders also the selection of a best functional in the presence of a kernel. Results for **1** and **2** are slightly deteriorated in the presence of the kernel. In view of the negligible dependence on EXX admixture, simple adjustment of the latter would not allow an improvement. For **3**, the computed shift decreases slightly more with larger EXX values, but good agreement with experiment (<10% deviation) would require 40% or more EXX admixture. Note that modelling of the lithium counter-ion interactions changes the shift only little (below 5 ppm). This contrasts to complex **4**, where the free anion has a much lower shift (by about −140 ppm, Fig. 4). The differences may be traced to an almost negligible change of the U–C bond length for **3** but a large increase for **4** (by 0.12 Å on average, Table S2, ESI†), emphasizing again the importance of structure. Increased shifts with larger EXX admixtures pertain to the more covalently bound complexes **4–7** (see above). While PBE0 provides excellent agreement with experiment for **5** and **6** (in fact better than PBE-40HF without kernel, Table 3), lower admixtures of around 10 and 15% would provide better agreement for **4** and **7**, respectively. The uncertainties of the interactions within the contact-ion pair **4** in the condensed-phase environment (see ref. 68 for solvent effects on ion-pair separation and $^{77}$Se and $^{125}$Te shifts in some thorium and uranium complexes), and the extreme structure dependence of the $^{13}$C shift (along with absence of an experimental structure) for **7** (Fig. 4) make the latter two systems less useful as benchmarks. Finally, the relatively modest SO contributions for **8** decrease with larger EXX admixture, and a value somewhat above the 25% of PBE0 would seem to provide best performance. We see therefore that the few available experimental data and a seemingly non-systematic behaviour render our choice of a functional clearly more difficult than for typical transition-metal hydride complexes.[7,14] A similarly difficult situation regarding the performance of DFT for ligand chemical shifts in actinide complexes has been identified for

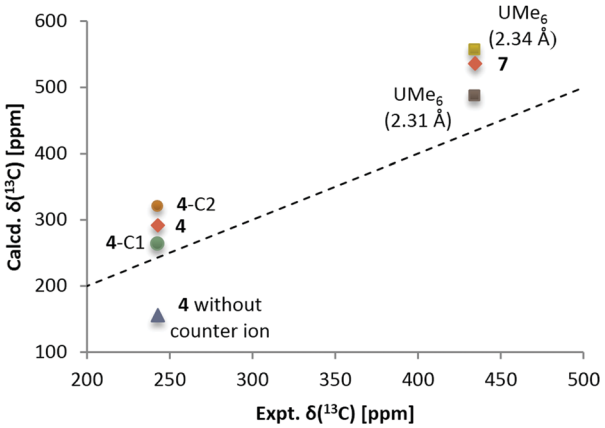


Fig. 4 Calculated $^{13}$C shifts with XC kernel and PBE0 functional compared to experiment for **4** and **7**. The dashed line represents ideal agreement with experiment. Cycles represent the two appreciably different calculated $^{13}$C shifts in **4** for two non-equivalent carbon atoms (the diamond gives the average). The triangle represents data for an anion-separated species of **4** ($[UO_2(CH_2SiMe_3)_4]^{2-}$), giving a much shielded carbon shift. Squares represent the truncated (hexamethyl) model **7′** with either PBE0-D3 optimized (2.34 Å) or artificially shortened (2.31 Å) U–C bonds. The extreme dependence on bond length may explain the overestimated shifts for the hexaalkyl complex **7** at PBE0 level.

$^{19}$F shifts of uranium fluoro–chloro complexes where, however, SO effects play no appreciable role.[69] Nevertheless, the standard functional PBE0 seems to perform overall well for the best-documented and -justified experimental values (Table 3, see also Fig. 5). While this level tends to overestimate the shifts somewhat for most of the complexes, it seems to be the best compromise for systems with a positive or negative dependence of the shift on EXX admixture (15% EXX would perform better for the former, 40% for the latter).

## Predictions of unknown $^{13}$C shift values in known organometallic uranium(VI) complexes

In an attempt to aid in widening the experimental database, Table 4 provides some $^{13}$C shift predictions for carbon atoms

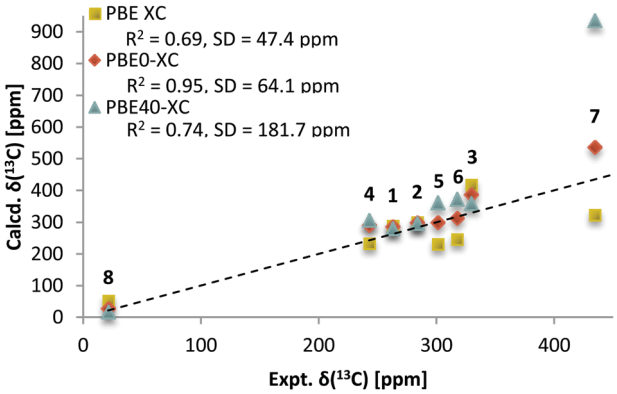


Fig. 5 Calculated $^{13}$C shifts with XC kernel and variable EXX admixture (yellow squares: 0%, red diamonds: 25%, blue triangles: 40%) compared to experiment for complexes **1–8** (*cf.* Table 3 for numerical values). The dashed line represents ideal agreement with experiment. Averaged data for two non-equivalent alkyl carbon atoms in **4** are shown.

bonded to a uranium(VI) center for the experimentally known complexes **9–14** (Fig. 6) where, however, the $^{13}$C signals so far could not be detected experimentally. As an overestimate is expected at the PBE0 level for those complexes, where the shifts decrease with increasing EXX admixture Table 4 contains also PBE-40HF results for these species. Together with the PBE results, the EXX dependence can again be extracted.

Complex **9** is electronically related to the NHC complexes **1** and **2**, and consequently the predicted $^{13}$C NMR shift for the U(VI)-bound carbon atoms is in the same range around 270 ppm (Table 4). It is unclear if attempts to measure this shift have been made.[70] In contrast, complexes **10–14** have been reported during the last 4 years. Together with **5** (*cf.* Fig. 1), Lewis *et al.*[65] also analysed the analogous alkinyl complex **10**. No $^{13}$C signal was found for the U(VI)-bound carbon atom. Given the good agreement of PBE0-XC data with experiment for **5** (Table 3), the predicted high-frequency shift of ~400 ppm at this level for **10** should be accurate. The larger value compared to **5** is not due to much larger SO shifts but caused by larger paramagnetic contributions (*cf.* Table S6 in ESI†). In fact, this increase is typical for going from an alkyl to an alkinyl ligand, more or less independently from the metal center.

Carbene complex **11** was analyzed[59] together with the structurally related methanide complex **8** which, however, has a much weaker and less covalent U–C interaction to the central carbon atom (*cf.* Table 5). The two complexes exhibit decreasing shift with increasing EXX admixture (Tables 3 and 4), with significantly larger SO effects and thus a larger shift for the carbene complex **11**. The PBE0 result of about 190 ppm can be expected to be slightly overestimated, our best prediction is thus closer to the PBE-40HF value of about 150 ppm. Increasing SO effects with larger EXX admixture are found for the related carbene complex **12** (Table 4). Due to very large paramagnetic and sizeable SO contributions a relatively high overall shift value of 370 ppm is predicted.

A much shorter U–C bond length in **12** compared to **11** (2.14 Å *vs.* 2.36 Å) is found, attributable to the well-known inverse *trans* influence (ITI) of the U=O bond.[68] No signal has been found experimentally, but the spectral region that was considered is unclear. In case of the related carbene complex **13**,[57] measurement ranged only up to 400 ppm. Here the calculations (on a slightly truncated model with methoxy for *t*-butoxy groups, changing the PBE-level shifts by only 12 ppm) predict a much larger carbon shift at the PBE0 level, with extremely large SO effects and a positive dependence on EXX admixture (Table 4). Even if the PBE0 value may overshoot notably in such cases (*cf.* **7** and **4** in Table 3), a $^{13}$C shift in the 550–620 ppm range seems likely. This prediction would not only be outside the measurement range but also provides a value at the very high-frequency end of known $^{13}$C shifts for a diamagnetic compound.[73,74] A re-measurement of **13**, possibly with a $^{13}$C-enriched carbene ligand, will be very interesting. However, we noted some irregularities for this complex in our computations: all optimized U–L bond-lengths for a singlet U(VI) ground-state differ notably from those found in the X-ray structure (*cf.* Tables S2 and S3 in ESI† and ref. 75), irrespective of the DFT functional, dispersion forces and alkoxy groups used

Table 4 Calculated $^{13}$C NMR shifts (in ppm *vs.* TMS; computed with XC kernel) for uranium-bonded carbon atoms in further synthetically known complexes (SO contributions in parentheses)[a]

| Complex | $\delta^{xc}_{2c}$ (PBE) | | $\delta^{xc}_{2c}$ (PBE0) | | $\delta^{xc}_{2c}$ (PBE-40HF) | | Exp. |
|---|---|---|---|---|---|---|---|
| **9** | 298.3 | (100.7) | 276.7 | (73.0) | 267.6 | (61.6) | [70,c] |
| **10** | 368.2 | (163.6) | 426.0 | (223.2) | — | — | [65,c] |
| **11** | 256.5 | (96.2) | 190.7 | (72.3) | 146.3 | (54.3) | [59,c] |
| **12** | 296.8 | (73.2) | 372.5 | (100.0) | — | — | [71,c] |
| **13**[b] | 417.4 | (164.5) | 702.1 | (390.5) | — | — | [58,d] |
| **14** | 278.0 | (76.6) | 220.4 | (59.0) | 179.9 | (46.0) | [72,e] |

[a] 2c-ZORA-SO results with TZ2P basis sets. See Fig. 6 for the structures of **9–14**. [b] Data computed for slightly truncated complex: O$^t$Bu replaced by OMe. [c] Spectral region of measurements unknown. [d] No signal found in the measurement range up to 400 ppm. [e] No signal found between −200 ppm and +1000 ppm.

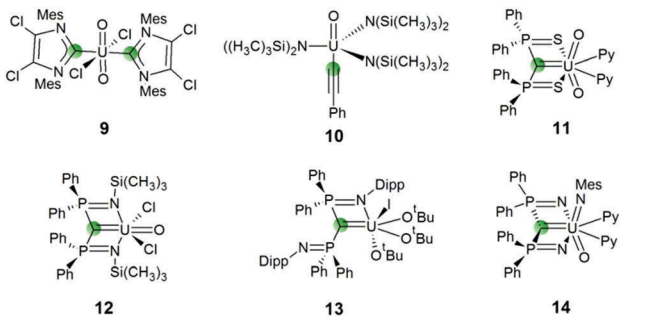


Fig. 6 Further experimentally known organometallic uranium(VI) complexes with undetermined $^{13}$C NMR shifts for uranium-bound carbon nuclei (highlighted in green).

Table 5 Quasi-relativistically optimized U–C distances, compositions of the U–C σ-bonding NLMOs, QTAIM delocalization indices (DI), and SO contributions to $^{13}$C shielding ($\sigma^{SO}$) for **1–14** (complexes are separated into two groups, where increasing EXX admixture decreases or increases the SO contributions to the shifts)[a]

| | $d$(U–C)[b] [Å] | NLMO[c] %U | %U(d) | %U(f) | %C | %C(s) | %C(p) | DI(U–C)[c] | $\sigma^{SO}$[d] |
|---|---|---|---|---|---|---|---|---|---|
| **1** | 2.63 | 16.4 | 49 | 32 | 79.9 | 44 | 56 | 0.366 | −77.7 |
| **2** | 2.61 | 14.9 | 47 | 33 | 80.7 | 40 | 60 | 0.374 | −62.2 |
| **3** | 2.48 | 22.2 | 43 | 40 | 75.0 | 40 | 60 | 0.550 | −169.0 |
| **8** | 2.64 | 15.3 | 49 | 43 | 75.4 | 8 | 92 | 0.420 | −12.6 |
| **9** | 2.61 | 16.3 | 47 | 32 | 80.6 | 44 | 56 | 0.387 | −72.1 |
| **11** | 2.36 | 21.5 | 52 | 42 | 70.2 | 20 | 80 | 0.792 | −71.4 |
| **14** | 2.37 | 20.9 | 47 | 49 | 69.7 | 18 | 82 | 0.779 | −58.2 |
| **4** | 2.46 | 22.1 | 34 | 53 | 74.6 | 22 | 78 | 0.644 | −212.0 |
| **5** | 2.30 | 28.5 | 24 | 73 | 66.0 | 25 | 75 | 0.869 | −171.9 |
| **6** | 2.28 | 27.7 | 25 | 72 | 64.7 | 20 | 80 | 0.937 | −136.5 |
| **7** | 2.32 | 28.7 | 25 | 68 | 69.2 | 22 | 78 | 0.844 | −362.7 |
| **10** | 2.29 | 28.9 | 34 | 60 | 68.2 | 49 | 51 | 0.767 | −222.3 |
| **12** | 2.14 | 30.8 | 21 | 77 | 62.7 | 18 | 82 | 1.224 | −99.1 |
| **13** | 2.22 | 28.2 | 26 | 68 | 67.7 | 31 | 69 | 1.251 | −390.0 |

[a] See Computational methods. The separation of the complexes into two groups is explained in the text. [b] Data for PBE0-D3 structures. [c] PBE0/ECP/TZVP results. [d] 2c-ZORA-SO/PBE0-XC/TZ2P results for U(VI)-bonded carbon atoms.

(*e.g.* the longest U–C bond found at the PBE/def2-TZVP level, $d$(U–C) = 2.32 Å, is still by 0.13 Å shorter than that found in the solid-state structure of **13**).

Excellent agreement between computed and experimental structure data for **13** was achieved by considering a triplet ground-state, revealing a U(IV) nature of the central metal in the X-ray structure.[75] This is also supported by the fact that the triplet U(IV) structure lies energetically lower than the corresponding closed-shell U(VI) structure by *ca.* 13 kJ mol$^{-1}$. Based on this small energetic gap, it is reasonable to assume that in solution the diamagnetic U(VI) complex **13** may exist in an equilibrium with the U(IV) species, as also supported by NMR data in ref. 58. The NMR spectra suggest the presence of a uranium-reduced "impurity" (tentatively assigned to a U(V) species) along with the diamagnetic U(VI) complex **13**. More detailed experimental studies might, however, be hindered due to instability of this complex, accompanied by the liberation of iodine.

Finally, the most recent carbene complex **14** in our selection exhibits a behaviour more similar to **11**: SO effects are more moderate and decrease with larger EXX admixture. A $^{13}$C shift near 180 ppm, similar to that predicted for **11**, seems most likely. In this case, the spectral range from −200 to +1000 ppm had been scanned without finding a $^{13}$C carbene signal.[72] It cannot be excluded that the shift may have fallen into the region of aromatic carbon atoms and thus gone unnoticed. As all of the non-detected actinide-bonded $^{13}$C shifts correspond to carbon atoms without hydrogen substituents, the missing signals could also be rationalized by their lower sensitivity (impossibility of direct $^{1}$H decoupling) and a $^{13}$C enrichment of the ligands would help to detect the corresponding signals.

### Rationalization of the observed trends by bonding analyses

To better understand the $^{13}$C shifts, their relation to the U–C bond for complexes **1–14**, and also the dependence of computed shifts (particularly their SO contributions) on the EXX admixture in the functional, we have carried out bonding analyses, looking in particular at natural localized molecular orbitals (NLMOs) obtained at scalar relativistic level (Table 5). For convenience, the entries in the Table are separated into those cases, where increasing EXX admixture decreases or increases the SO contributions to the shifts (first and second group of complexes).

The longest U–C bonds (single bonds in **1**, **2**, **4**, **8**, **9**, an NHC "single bond" in **3**, and comparably long carbene double bonds in **11**, **14**) pertain generally to carbon atoms in equatorial position to a uranyl $UO_2^{2+}$ unit (or to an isoelectronic $UON^{+}$ moiety in **14**). Much shorter U–C bonds (Table 5) are found for systems with the carbon ligand in *trans* position with respect to an U=O bond (ITI: **5**, **6**, **10**, particularly the double bond in **12**) or for those, which possess no competing strong π-donor ligand (hexaalkyl complex **7** and carbene complex **13**, where the carbene ligand is the only strong π-donor). The bond lengths correlate closely with covalency, as indicated by the percentage uranium character (%U) in the corresponding σ-bonding NLMO (Table 5, plotted separately for U–C and U=C bonds in Fig. 7).

The separation made in Table 5 between complexes with negative and positive dependence of their (absolute) SO

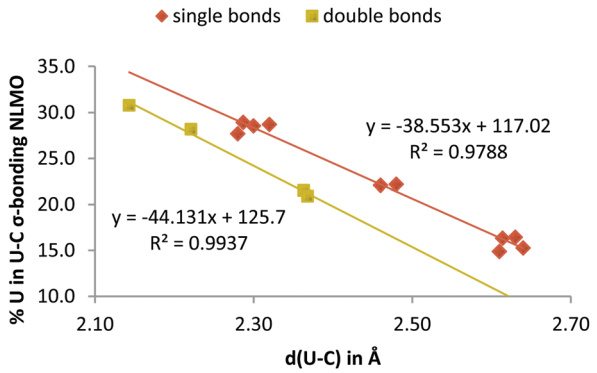


Fig. 7 Correlation between total uranium involvement in the U–C σ-bonding NLMO with U–C bond length, with separate regression lines for U–C single bonds (**1–10**, red diamonds) and carbene U=C double bonds (**11–14**, yellow squares). NHC complex **3** has been plotted with the single-bonded species.

contributions to the $^{13}$C shifts on EXX admixture in the functional (*cf.* Tables 1, 3 and 4) can therefore be related to the position of the carbon atom in the complex: positions equatorial to an uranyl (or related) unit lead to a negative dependence, positions *trans* to a U=O bond or the absence of competing strong π-donor ligands in the system give a positive dependence. The recent uranyl-tetraalkyl "ate" complex **4** is the only exception to this rule and provides a borderline case: even though the alkyl ligands are positioned equatorially to a uranyl unit, their U–C bonds still have appreciable covalency (see NLMO composition and QTAIM delocalization index, DI, in Table 5), and the absolute SO contributions exhibit a positive dependence on EXX admixture (Tables 1 and 3).

Further insights are provided by analyzing the overall 5f- *vs.* 6d-orbital involvement in the U–C σ-bonding NLMO. This is shown in Fig. 8, which is ordered by increasing 5f-orbital involvement. Indeed, this ordering separates the investigated complexes into exactly the same groups as we chose for Table 5: the more covalent complexes clearly exhibit dominant 5f-orbital character of the U–C σ-bond (right side of Fig. 8), whereas the 6d-orbital character is comparably small here. In contrast, the less covalent complexes display clearly diminished 5f-orbital character and larger 6d contributions. Uranyl-tetraalkyl complex **4** is just on the borderline where the uranium 5f-orbitals start to make up more than 10% of the overall σ-bonding NLMO.

We may use this observation to provide a tentative rationalization of the at first sight non-systematic dependence of the SO-shifts on EXX admixture. Increasing EXX admixture renders the metal ligand bonds generally less covalent, due to reduction of self-interaction errors ("delocalization errors") in the functional (this is well-known also for transition-metal complexes).[76,77] For the less covalent cases (with predominantly equatorial position to a uranyl unit), the 6d-orbital character dominates the uranium contributions to the U–C σ-bond, and the 5f-orbital involvement is small. In these bonds increasing EXX admixture diminishes the SO contributions to the $^{13}$C by interrupting the Fermi-contact pathway that transmits the SO-induced spin polarization from the heavy uranium center to the carbon nucleus.[3] In contrast, for the more covalent cases with dominant uranium 5f-orbital

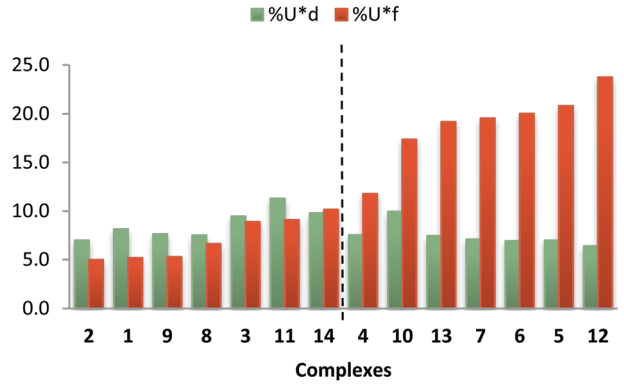


Fig. 8 Total d and f orbital involvement (uranium percentage in the U–C bonding times given orbital type contribution) in the U–C σ-bonding NLMO ordered by increasing f orbital contributions.

contributions to the bond, the possible main effects of larger EXX admixture are (a) increased SO matrix elements due to the larger uranium 5f-character of the MOs, and (b) increased SO terms due to enhanced polarization with larger EXX admixture. We have confirmed these assumptions by a computational experiment in which a finite Fermi-contact perturbation is placed at the carbon nucleus (such perturbations are often used for perturbational computations of SO shifts[5,6,11] or of spin–spin coupling constants[78]), and the delocalization of the induced spin density throughout the system is monitored as a function of EXX admixture (comparing PBE, PBE0, PBE-40HF functionals). The results are provided in ESI† (Table S13 gives Mulliken atomic spin densities and Fig. S1 isosurface plots of the induced spin density). Larger EXX admixture reduces the induced spin density at uranium for **3**, consistent with lowered SO-contributions to the shifts for this complex. In contrast, **4** represents the second class of complexes, where larger EXX admixture enhances the SO shifts, and indeed the induced spin density at uranium increases in this case, consistent with the abovementioned increased polarization.

While these analyses allow us to understand the dependence of SO shifts on EXX admixture, we still need to provide some appreciation of the rather large variations of SO shifts, and of $^{13}$C shifts in general, for the different complexes. The 5f-orbital covalency arguments and position of the carbon ligand relative to strong π-donor ligands in a given complex, as discussed above, give a general framework, as roughly speaking the overall SO shifts are larger for the complexes in the second (bottom) half of Table 5 compared to the first (upper) half. However, to understand the trends in more detail, other aspects have to be considered as well: the by far largest SO shifts (and the largest dependence on the functional) are found for carbene complex **13** and hexaalkyl complex **7** (Table 5). These two systems share the absence of other strong π-donor ligands in the complex and are obviously at the limits of stability of U(VI) complexes (see also discussion above). This is for instance reflected by the relatively small HOMO–LUMO gap of **13** (2.1 eV at PBE0/TZ2P level), only half of that for the other complexes. This gives rise to relatively small energy denominators, enhancing the SO contributions as well as the paramagnetic contributions which are particularly large as well (Table 4). **7** does not exhibit a conspicuously small HOMO–LUMO gap but a relatively large uranium 5f-orbital and simultaneously large carbon AO participation in the three highest occupied and also in the low-lying virtual MOs. This enhances in particular the SO contributions to the NMR shielding.

Among the first group of complexes in Table 5, **3** features the by far largest overall SO shifts (even though they decrease with increasing EXX admixture, see above). This seems to be due to a comparably small HOMO–LUMO gap in combination with high uranium 5f-character and equally high carbon 2s-character in the U–C bond to this NHC ligand, in spite of the equatorial position to a uranyl group, which overall diminishes the U–C bond covalency. **3** may be contrasted against the carbene complexes **11** and **14** (the latter two possessing a double-bond U═C character), which feature shorter U–C bonds and even larger covalency but much smaller SO shifts (Table 5). Here the low carbon 2s-character in the U–C bond of only about 20% compared to 40% in **3** is particularly notable. Caused by the large P–C–P angle of this type of pincer carbene ligand (149° and 150° for **11** and **14**, respectively), the low carbon 2s-character in the bond reduces the effectiveness of the Fermi-contact mechanism for transferring SO-induced spin polarization to the carbon nucleus.[3] This effect is even more notable for the methanide complex **8**: while its overall covalency (%U character and DI in Table 5) is not much lower than for the other complexes in the first group in Table 5, the carbon 2s-character of only 8% in the σ-bonding NLMO signals a particularly poor Fermi-contact spin-density transfer and thus explains the smallest SO shifts in the entire set of complexes studied here. The different influences may also compensate to the extent that similar SO shifts arise for rather different bonding situations. For example, the equatorial imidazolyl ligands in **1**, **2**, **9** feature relatively long U–C bonds with low covalency and uranium 5f-character in the bond, but carbon 2s-contributions of about 40%. They have similar SO shifts as the much more covalent complexes **11**, **14** (featuring much larger uranium 5f-character in the σ-bonding NLMO), due to the abovementioned low carbon 2s-character of only about 20% for these pincer carbene complexes.

Most of the complexes of the second group (Table 5) have very large SO shifts in spite of carbon 2s-contributions of only about 20%. Here it is clearly the large covalency and uranium 5f-character in the bond and relatively high-lying occupied MOs that cause the large SO effects. In analogy to complex **8** the carbene complex **12** exhibits comparably low carbon 2s-character due to the pincer-type geometry and consequently has the clearly lowest SO shifts in the second group of complexes. The acetylide complex **10** represents an outlier: it naturally exhibits particularly large carbon 2s-character in the bond but somewhat diminished uranium 5f-character. In fact, the large carbon 2s-character in the C–U bond in **10** causes the associated canonical MOs (mostly HOMO−11, compared to HOMO−3 for **5**) to be very low in energy, leading to relatively large energy denominators in the perturbation expressions, and thus diminished SO contributions.

 

### Revised predictions of $^1$H shifts in uranium(VI) hydride complexes

The main goal of ref. 12 had been the prediction of $^1$H shifts of hypothetical uranium(VI) hydride complexes, based on the method calibration done for known $^{13}$C values. Using PBE-40HF without kernel as "best functional" then led to the prediction[12] of record high-frequency $^1$H shifts for so far unknown uranium(VI) hydride complexes, far above the highest-frequency $^1$H shifts around 20 ppm for diamagnetic compounds.[13] Here we thus have to re-examine these predictions in light of the missing XC kernel in the older ADF implementation (see Fig. 9 for the selected systems, encompassing both unrealistic small models and more realistic target complexes for potential synthesis). We now use consistently PBE0-D3 structures, and thus even PBE-40HF results without kernel deviate somewhat from the values in ref. 12 (by about 4 ppm). Table 6 compares these data with PBE and PBE0 2-component ZORA and PBE 4-component mDKS results, all including a proper kernel treatment. As the U–H bonds exhibit similar covalent bonding character as the σ-bonded U–C bonds above, it is no surprise that the kernel contributions increase the $^1$H shifts appreciably for a given functional (see Table S14 in ESI†). And as in the abovementioned $^{13}$C cases, the effect of the kernel is largest for the overall largest shifts.[12] Dependence of the $^1$H SO shifts also follows the same patterns as analysed above for the $^{13}$C shifts: hydrides in equatorial position to a uranyl or related RN═U═NR moiety exhibit decreasing absolute SO shifts with increasing EXX admixture (**18–22**), whereas the opposite trend is found for complexes with a hydride ligand in *trans* position to a U═O bond (**23**) or in the absence of a strong π-donor ligand (**15–17**). The synthetically less likely model complexes **15–17** without strong π-donors exhibit the same large sensitivity to the input structure (Table S15, ESI†) and EXX admixture as complex **7** above. Here we may expect that PBE0 calculations with kernel may overshoot significantly. However, even if we take the PBE values as lower bound, extremely large $^1$H shifts between 170 ppm for **16**, **17** and 265 ppm for **15** are predicted far outside the known $^1$H shift range of diamagnetic compounds.

The hypothetical uranium(VI) hydride **23** is closely related to complexes **5** and **6** (and **10**; *cf.* Fig. 1, 6, and 9), and we may expect similar performance of our methodology as for the $^{13}$C shifts in these systems, where PBE0 with kernel provided excellent agreement with experiment. We thus regard the predicted $^1$H shift of about +170 ppm (with almost the same magnitude of the SO contributions; Table 6) as accurate. Given the ITI provided by the *trans* U═O group,[65] **23** may be a particularly promising target system and would already extend the known $^1$H shift range dramatically!

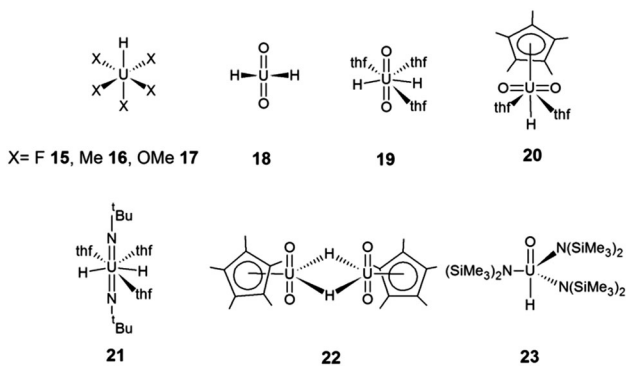


Fig. 9 Model uranium(VI) hydrides.

Table 6 Predicted hydride $^1$H NMR shifts (*vs.* TMS in ppm) for uranium(VI) hydride complexes. SO contributions are given in parentheses[a]

| | $\delta_{2c}$ (PBE-40HF) | | $\delta_{2c}^{xc}$ (PBE) | | $\delta_{2c}^{xc}$ (PBE0) | | $\delta_{4c}^{xc}$ (PBE) |
|---|---|---|---|---|---|---|---|
| **15** | 443.4 | (445.6) | 265.5 | (263.7) | 603.7 | (606.8) | 251.8 |
| **16** | 267.3 | (253.8) | 171.0 | (153.4) | 336.6 | (321.1) | 163.8 |
| **17** | 282.2 | (280.2) | 178.4 | (172.6) | 348.8 | (346.2) | 174.0 |
| **18** | 55.7 | (42.3) | 132.2 | (120.7) | 87.3 | (74.3) | 136.9 |
| **19** | 90.7 | (81.6) | 212.1 | (207.8) | 163.4 | (156.2) | 209.4 |
| **20** | 58.1 | (45.3) | 93.9 | (84.7) | 83.2 | (71.5) | 95.4 |
| **21** | 60.2 | (48.7) | 124.8 | (114.0) | 84.1 | (72.2) | 122.6 |
| **22** | 39.0 | (26.6) | 55.6 | (50.4) | 49.8 | (39.6) | 57.3 |
| **23** | 142.5 | (144.5) | 117.6 | (108.5) | 170.5 | (169.1) | 115.2 |

[a] 2c-ZORA-SO/TZ2P results (see Computational details).

As **18** and the more realistic target complexes **19–22** exhibit smaller sensitivity to the input structure and decreasing SO-shifts with increasing EXX admixture (comparable to the $^{13}$C shifts of **3** above, *cf.* Table 3), we may expect to overshoot the $^1$H shifts somewhat at PBE0 level, approaching the exact value from above with increased EXX admixture. In keeping with our analyses for the $^{13}$C shift cases (**1–3**, **8**, **9**, **11**, **14**) above, less dramatic high-frequency shifts in the range of about 30–70 ppm are expected for these equatorial hydrides, albeit still generally far above the known $^1$H shift range. Among these five complexes, **19** is a clear outlier, predicted to have a much larger shift than the other four systems.

PBE0 with kernel generally provides larger hydride $^1$H shifts for all complexes in Table 6 than PBE-40HF without kernel. As the electronic structure of these hydride complexes suggests that PBE0 with kernel may actually overshoot somewhat in most cases, in particular for the equatorial hydrides (**23** may be an exception, where PBE0 with kernel should be more accurate), our previous predictions[12] seem reasonable, even though they had been obtained by a fortuitous compensation between missing kernel and too large EXX admixture. In any case the prediction of unprecedented high-frequency $^1$H shift ranges for uranium(VI) hydride complexes is upheld, and we can place substantially more confidence into these predictions than hitherto, as we better understand the interplay between molecular and electronic structure and functional. We finally note again the very good agreement between 2-component ZORA and 4-component mDKS results at PBE level when the XC response kernel contributions to the shielding are either included or neglected in both approaches (Table 2).

### Chemical-shift anisotropies

Tables S16 and S17 in ESI† provide the computed principal components of $^{13}$C and $^1$H shift tensors (PBE0 level with kernel), respectively, for the complexes studied in this work.

The results confirm our expectation of very large shift anisotropies in many cases, in particular for those species where SO effects lead also to particularly large isotropic shifts (the anisotropy values range from several tens of ppm up to about 700 ppm for both $^{1}$H and $^{13}$C nuclei).

These shift tensors could be probed by suitable solid-state experiments in the future. Notably, very large chemical-shift anisotropies (CSAs) could lead to fast relaxation processes, in particular in solution.[79,80] This could also explain some of the "non-observed" $^{13}$C signals for carbon nuclei directly bound to uranium in some of the synthetically known complexes. Possibly, this could also have been a reason for a lack of observation of $^{1}$H signals for uranium(VI) hydride complexes. In any case, CSA-induced relaxation processes may have to be kept in mind in experimental studies of such species.

## Conclusions

While our previous predictions of giant $^{1}$H NMR shifts in closed-shell uranium(VI) hydride complexes and of also extremely large spin–orbit-induced $^{13}$C shifts for uranium(VI)-bound carbon atoms had been obtained without consideration of the exchange–correlation kernel in two-component ZORA DFT calculations, our present study confirms these unusual predictions when the kernel is properly accounted for. The EXX admixture needed to reproduce known spin–orbit-dominated $^{13}$C shifts in such species is then reduced considerably, compared to the previous study, from about 40% without kernel to a compromise value closer to 25% with kernel. The overall predicted range for unknown shifts with the revised approach is retained. That is, we still predict $^{1}$H hydride shifts in uranium(VI) hydride complexes between 30 ppm and more than 200 ppm, maybe up to 170 ppm for the most realistic target complexes. This is clearly outside the known $^{1}$H shift range for diamagnetic systems. Very large spin–orbit induced $^{13}$C shifts for uranium-bound carbon atoms are also confirmed, and predictions have been made for complexes that are synthetically known, but where these carbon shifts so far had not been found. In one known pincer carbene complex, an extremely large shift beyond 550 ppm has been predicted.

The present analyses provide much tighter confidence ranges for the predicted shifts than obtained previously, due to improved understanding achieved for dependences on structure, bonding type, and functional. Notably, we find appreciable dependencies on (a) the overall covalency of the U–C bond, (b) the uranium 5f-orbital character in the bond, but also (c) the carbon 2s-contributions to the bonding NLMO. While the latter aspect may be rationalized by known Fermi-contact-type mechanisms for SO-induced shifts, the 5f-participation is crucial due to SO matrix elements. We find furthermore a clear dependence on the position of the carbon atom in question within a given complex: equatorial positions relative to strong π-donor uranyl or related groups lead to a negative dependence of absolute SO-shifts on EXX admixture in the functional (further insights into these aspects have also been provided) and tend to generally reduce covalency and shifts. Particularly large NMR shifts are found in the absence of strong π-donor ligands in the complex (unfortunately for the possible identification of uranium(VI) hydrides, this will likely also render the complexes less stable) and also for U–C or U–H bonds in *trans* position to a U═O bond. These qualitative findings should enable a more meaningful design, and will help also in the experimental characterization of suitable target complexes by NMR spectroscopy.

## Acknowledgements

AHG thanks Fonds der chemischen Industrie for a PhD scholarship. Funding from the Berlin DFG excellence cluster on Unifying Concepts in Catalysis is gratefully acknowledged. JA acknowledges support from the U.S. Department of Energy, Office of Basic Energy Sciences, Heavy Element Chemistry program, under grant DE-SC0001136 (formerly DE-FG02-09ER16066).

## References

1 P. Pyykkö, A. Görling and N. Rösch, *Mol. Phys.*, 1987, **61**, 195–205.
2 M. Kaupp, in *Relativistic Electronic Structure Theory II: Applications*, ed. P. Schwerdtfeger, Elsevier, Amsterdam, 2004, pp. 552–597.
3 M. Kaupp, O. L. Malkina, V. G. Malkin and P. Pyykkö, *Chem. – Eur. J.*, 1998, **4**, 118–126.
4 Y. Nomura, Y. Takeuchi and N. Nakagawa, *Tetrahedron Lett.*, 1969, **10**, 639–642.
5 O. L. Malkina, B. Schimmelpfennig, M. Kaupp, B. A. Hess, P. Chandra, U. Wahlgren and V. G. Malkin, *Chem. Phys. Lett.*, 1998, **296**, 93–104.
6 V. G. Malkin, O. L. Malkina and D. R. Salahub, *Chem. Phys. Lett.*, 1996, **261**, 335–345.
7 P. Hrobárik, V. Hrobáriková, F. Meier, M. Repiský, S. Komorovský and M. Kaupp, *J. Phys. Chem. A*, 2011, **115**, 5654–5659.
8 P. Garbacz, V. V. Terskikh, M. J. Ferguson, G. M. Bernard, M. Kędziorek and R. E. Wasylishen, *J. Phys. Chem. A*, 2014, **118**, 1203–1212.
9 A. Bagno and G. Saielli, *Phys. Chem. Chem. Phys.*, 2011, **13**, 4285–4291.
10 M. Kaupp and O. L. Malkina, *J. Chem. Phys.*, 1998, **108**, 3648–3659.
11 J. Vaara, O. L. Malkina, H. Stoll, V. G. Malkin and M. Kaupp, *J. Chem. Phys.*, 2001, **114**, 61–71.
12 P. Hrobárik, V. Hrobáriková, A. H. Greif and M. Kaupp, *Angew. Chem., Int. Ed.*, 2012, **51**, 10884–10888.
13 B. C. Parkin, J. R. Clark, V. M. Visciglio, P. E. Fanwick and I. P. Rothwell, *Organometallics*, 1995, **14**, 3002–3013.
14 A. H. Greif, P. Hrobárik, V. Hrobáriková, A. V. Arbuznikov, J. Autschbach and M. Kaupp, *Inorg. Chem.*, 2015, **54**, 7199–7208.
15 J. Vícha, J. Novotný, M. Straka, M. Repisky, K. Ruud, S. Komorovsky and R. Marek, *Phys. Chem. Chem. Phys.*, 2015, **17**, 24944–24955.
16 S. K. Wolff and T. Ziegler, *J. Chem. Phys.*, 1998, **109**, 895–905.
17 S. K. Wolff, T. Ziegler, E. van Lenthe and E. J. Baerends, *J. Chem. Phys.*, 1999, **110**, 7689–7698.

 

18 L. A. Seaman, P. Hrobárik, M. F. Schettini, S. Fortier, M. Kaupp and T. W. Hayton, *Angew. Chem., Int. Ed. Engl.*, 2013, **52**, 3259–3263.
19 Amsterdam Density Functional (ADF) version 2012.01, SCM, Theoretical Chemistry, Vrije Universiteit, Amsterdam, Netherlands, 2012, available from http://www.scm.com.
20 J. Autschbach, *Mol. Phys.*, 2013, **111**, 2544–2554.
21 S. Komorovský, M. Repiský, O. L. Malkina, V. G. Malkin, I. Malkin Ondík and M. Kaupp, *J. Chem. Phys.*, 2008, **128**, 104101.
22 A. Wodyński, M. Repiský and M. Pecul, *J. Chem. Phys.*, 2012, **137**, 14311.
23 V. Arcisauskaite, J. I. Melo, L. Hemmingsen and S. P. A. Sauer, *J. Chem. Phys.*, 2011, **135**, 44306.
24 S. Komorovsky, M. Repisky, K. Ruud, O. L. Malkina and V. G. Malkin, *J. Phys. Chem. A*, 2013, **117**, 14209–14219.
25 *Turbomole, version 6.3.1*, a development of University of Karlsruhe and Forschungszentrum Karlsruhe GmbH, 1989-2007, TURBOMOLE GmbH, since 2007, available from http://www.turbomole.com.
26 X. Cao and M. Dolg, *THEOCHEM*, 2004, **673**, 203–209.
27 F. Weigend and R. Ahlrichs, *Phys. Chem. Chem. Phys.*, 2005, **7**, 3297–3305.
28 J. P. Perdew, K. Burke and M. Ernzerhof, *Phys. Rev. Lett.*, 1997, **78**, 1396.
29 J. P. Perdew and Y. Wang, *Phys. Rev. B: Condens. Matter Mater. Phys.*, 1992, **45**, 13244–13249.
30 A. D. Becke, *Phys. Rev. A: At., Mol., Opt. Phys.*, 1988, **38**, 3098–3100.
31 C. Lee, W. Yang and R. G. Parr, *Phys. Rev. B: Condens. Matter Mater. Phys.*, 1988, **37**, 785–789.
32 S. Grimme, S. Ehrlich and L. Goerigk, *J. Comput. Chem.*, 2011, **32**, 1456–1465.
33 S. Grimme, J. Antony, S. Ehrlich and H. Krieg, *J. Chem. Phys.*, 2010, **132**, 154104.
34 M. Ernzerhof and G. E. Scuseria, *J. Chem. Phys.*, 1999, **110**, 5029–5036.
35 S. Grimme, *J. Comput. Chem.*, 2004, **25**, 1463–1473.
36 D. N. Laikov, *Chem. Phys. Lett.*, 1997, **281**, 151–156.
37 A. E. Hansen and T. D. Bouman, *J. Chem. Phys.*, 1985, **82**, 5035–5047.
38 S. H. Vosko, L. Wilk and M. Nusair, *Can. J. Phys.*, 1980, **58**, 1200–1211.
39 A. Klamt and V. Jonas, *J. Chem. Phys.*, 1996, **105**, 9972–9981.
40 A. Klamt, *J. Phys. Chem.*, 1995, **99**, 2224–2235.
41 A. Klamt and G. Schüürmann, *J. Chem. Soc., Perkin Trans. 2*, 1993, 799–805.
42 ReSpect, version 3.4.2 (2015) – Relativistic Spectroscopy DFT program of authors M. Repisky, S. Komorovsky, V. G. Malkin, O. L. Malkina, M. Kaupp and K. Ruud, with contributions from R. Bast, U. Ekstrom, M. Kadek, S. Knecht, L. Konečný, E. Malkin and I. Malkin-Ondík, see http://www.respectprogram.org.
43 G. A. Aucar, T. Saue, L. Visscher and H. J. A. Jensen, *J. Chem. Phys.*, 1999, **110**, 6208–6218.
44 W. Kutzelnigg, *J. Comput. Chem.*, 1999, **20**, 1199–1219.
45 C. Adamo and V. Barone, *Chem. Phys. Lett.*, 1998, **298**, 113–119.
46 K. G. Dyall, *Theor. Chem. Acc.*, 2007, **117**, 491–500.
47 W. Kutzelnigg, U. Fleischer and M. Schindler, *NMR—Basic Principles and Progress*, Springer Verlag, Berlin, 23rd edn, 1991, p. 165.
48 M. J. Frisch, G. W. Trucks, H. B. Schlegel, G. E. Scuseria, M. A. Robb, J. R. Cheeseman, G. Scalmani, V. Barone, B. Mennucci, G. A. Petersson, H. Nakatsuji, M. Caricato, X. Li, H. P. Hratchian, A. F. Izmaylov, J. Bloino, G. Zheng, J. L. Sonnenberg, M. Hada, M. Ehara, K. Toyota, R. Fukuda, J. Hasegawa, M. Ishida, T. Nakajima, Y. Honda, O. Kitao, H. Nakai, T. Vreven, J. A. Montgomery, Jr., J. E. Peralta, F. Ogliaro, M. Bearpark, J. J. Heyd, E. Brothers, K. N. Kudin, V. N. Staroverov, R. Kobayashi, J. Normand, K. Raghavachari, A. Rendell, J. C. Burant, S. S. Iyengar, J. Tomasi, M. Cossi, N. Rega, J. M. Millam, M. Klene, J. E. Knox, J. B. Cross, V. Bakken, C. Adamo, J. Jaramillo, R. Gomperts, R. E. Stratmann, O. Yazyev, A. J. Austin, R. Cammi, C. Pomelli, J. W. Ochterski, R. L. Martin, K. Morokuma, V. G. Zakrzewski, G. A. Voth, P. Salvador, J. J. Dannenberg, S. Dapprich, A. D. Daniels, O. Farkas, J. B. Foresman, J. V. Ortiz, J. Cioslowski and D. J. Fox, *Gaussian 09, revision A.02*, Gaussian, Inc., Wallingford CT, 2009.
49 A. Schäfer, C. Huber and R. Ahlrichs, *J. Chem. Phys.*, 1994, **100**, 5829–5835.
50 X. Cao, M. Dolg and H. Stoll, *J. Chem. Phys.*, 2003, **118**, 487–495.
51 E. D. Glendening, J. K. Badenhoop, A. E. Reed, J. E. Carpenter, J. A. Bohmann, C. M. Morales, F. Weinhold, *NBO 5.0*, Theoretical Chemistry Institute, University of Wisconsin, Madison, 2001.
52 E. D. Glendening, J. K. Badenhoop, A. E. Reed, J. E. Carpenter, J. A. Bohmann, C. M. Morales, C. R. Landis and F. Weinhold, *NBO, versions 5.9 and 6.0*, Theoretical Chemistry Institute, University of Wisconsin, Madison, WI, 2013, available from http://nbo.chem.wisc.edu.
53 R. F. W. Bader, *Atoms in molecules: a quantum theory*, Clarendon Press, Oxford University Press, Oxford, New York, 1994.
54 R. F. W. Bader and M. E. Stephens, *J. Am. Chem. Soc.*, 1975, **97**, 7391–7399.
55 T. Lu, Multiwfn*: A Multifunctional Wave Function Analyzer, version 3.3.7*, 2015, available from http://multiwfn.codeplex.com.
56 T. Lu and F. Chen, *J. Comput. Chem.*, 2012, **33**, 580–592.
57 S. T. Liddle, *Angew. Chem., Int. Ed. Engl.*, 2015, **54**, 8604–8641.
58 O. J. Cooper, D. P. Mills, J. McMaster, F. Tuna, E. J. L. McInnes, W. Lewis, A. J. Blake and S. T. Liddle, *Chem. – Eur. J.*, 2013, **19**, 7071–7083.
59 J.-C. Tourneux, J.-C. Berthet, T. Cantat, P. Thuéry, N. Mézailles and M. Ephritikhine, *J. Am. Chem. Soc.*, 2011, **133**, 6162–6165.
60 M. J. Sarsfield, H. Steele, M. Helliwell and S. J. Teat, *Dalton Trans.*, 2003, 3443–3449.
61 J. Autschbach and T. Ziegler, *J. Chem. Phys.*, 2000, **113**, 9410–9418.
62 P. L. Arnold, I. J. Casely, Z. R. Turner and C. D. Carmichael, *Chem. – Eur. J.*, 2008, **14**, 10415–10422.
63 S. A. Mungur, S. T. Liddle, C. Wilson, M. J. Sarsfield and P. L. Arnold, *Chem. Commun.*, 2004, 2738–2739.

64 M. F. Schettini, G. Wu and T. W. Hayton, *Chem. Commun.*, 2012, **48**, 1484–1486.
65 A. J. Lewis, P. J. Carroll and E. J. Schelter, *J. Am. Chem. Soc.*, 2013, **135**, 13185–13192.
66 S. Fortier, N. Kaltsoyannis, G. Wu and T. W. Hayton, *J. Am. Chem. Soc.*, 2011, **133**, 14224–14227.
67 S. Fortier, J. R. Walensky, G. Wu and T. W. Hayton, *J. Am. Chem. Soc.*, 2011, **133**, 11732–11743.
68 D. E. Smiles, G. Wu, P. Hrobárik and T. W. Hayton, *J. Am. Chem. Soc.*, 2016, **138**, 814–825.
69 M. Straka and M. Kaupp, *Chem. Phys.*, 2005, **311**, 45–56.
70 W. J. Oldham Jr., S. M. Oldham, W. H. Smith, D. A. Costa, B. L. Scott and K. D. Abney, *Chem. Commun.*, 2001, 1348–1349.
71 D. P. Mills, O. J. Cooper, F. Tuna, E. J. L. McInnes, E. S. Davies, J. McMaster, F. Moro, W. Lewis, A. J. Blake and S. T. Liddle, *J. Am. Chem. Soc.*, 2012, **134**, 10047–10054.
72 E. Lu, O. J. Cooper, J. McMaster, F. Tuna, E. J. L. McInnes, W. Lewis, A. J. Blake and S. T. Liddle, *Angew. Chem., Int. Ed.*, 2014, **53**, 6696–6700.
73 J. Vícha, R. Marek and M. Straka, *Inorg. Chem.*, 2016, **55**, 1770–1781.
74 S. Takemoto, J. Ohata, K. Umetani, M. Yamaguchi and H. Matsuzaka, *J. Am. Chem. Soc.*, 2014, **136**, 15889–15892.
75 PBE0-D3/def2-TZVP optimized bond-lengths in complex **13** considering a singlet U(VI) ground-state: $d$(U–C) = 2.22 Å, $d$(U–N) = 2.26 Å, $d(\text{U–O})_{\text{avg.}}$ = 2.01 Å, $d$(U–I) = 3.03 Å; PBE0-D3/def2-TZVP optimized bond-lengths in complex **13** considering a triplet U(IV) ground-state: $d$(U–C) = 2.44 Å, $d$(U–N) = 2.36 Å, $d(\text{U–O})_{\text{avg.}}$ = 2.04 Å, $d$(U–I) = 3.10 Å; X-ray structure data: $d$(U–C) = 2.45 Å, $d$(U–N) = 2.36 Å, $d(\text{U–O})_{\text{avg.}}$ = 2.05 Å, $d$(U–I) = 3.11 Å.
76 M. Kaupp, R. Reviakine, O. L. Malkina, A. Arbuznikov, B. Schimmelpfennig and V. G. Malkin, *J. Comput. Chem.*, 2002, **23**, 794–803.
77 J. Autschbach and M. Srebro, *Acc. Chem. Res.*, 2014, **47**, 2592–2602.
78 V. G. Malkin, O. L. Malkina and D. R. Salahub, *Chem. Phys. Lett.*, 1994, **221**, 91–99.
79 R. E. Wasylishen, G. L. Neufeld and K. J. Friesen, *Inorg. Chem.*, 1981, **20**, 637–638.
80 B. E. Eichler, B. L. Phillips, P. P. Power and M. P. Augustine, *Inorg. Chem.*, 2000, **39**, 5450–5453.

 